The Role of Homophilic Binding in Anti-tumor Antibody R24 Recognition of Molecular Surfaces

DEMONSTRATION OF AN INTERMOLECULAR β-SHEET INTERACTION BETWEEN V_H DOMAINS*

Marcin J. Kaminski‡, C. Roger MacKenzie§, Marilyn J. Mooibroek‡, Tanya E. S. Dahms‡, Tomoko Hirama§, Alan N. Houghton¶, Paul B. Chapman¶, and Stephen V. Evans‡‖

From the ‡Department of Biochemistry, University of Ottawa, Ottawa, Ontario K1H 8M5, Canada, the §Institute for Biological Sciences, National Research Council of Canada, Ottawa, Ontario K1A 0R6, Canada, and the ¶Memorial Sloan-Kettering Cancer Center, New York, New York 10021

The murine antibody R24 and mouse-human Fv-IgG1(κ) chimeric antibody chR24 are specific for the cell-surface tumor antigen disialoganglioside GD3. X-ray diffraction and surface plasmon resonance experiments have been employed to study the mechanism of "homophilic binding," in which molecules of R24 recognize and bind to other molecules of R24 though their heavy chain variable domains. R24 exhibits strong binding to liposomes containing disialoganglioside GD3; however, the kinetics are unusual in that saturation of binding is not observed. The binding of chR24 to GD3-bearing liposomes is significantly weaker, suggesting that cooperative interactions involving antibody constant regions contribute to R24 binding of membrane-bound GD3. The crystal structures of the Fabs from R24 and chR24 reveal the mechanism for homophilic binding and confirm that the homophilic and antigen-binding idiotopes are distinct. The homophilic binding idiotope is formed largely by an anti-parallel β-sheet dimerization between the H2 complementarity determining region (CDR) loops of two Fabs, while the antigen-binding idiotope is a pocket formed by the three CDR loops on the heavy chain. The formation of homophilic dimers requires the presence of a canonical conformation for the H2 CDR in conjunction with participation of side chains. The relative positions of the homophilic and antigen-binding sites allows for a lattice of GD3-specific antibodies to be constructed, which is stabilized by the presence of the cell membrane. This model provides for the selective recognition by R24 of cells that overexpress GD3 on the cell surface.

Immunotherapy using monoclonal antibodies (mAbs)[1] to tar-

‖ To whom correspondence should be addressed: Dept. of Biochemistry, University of Ottawa, 451 Smyth, Ottawa, Ontario K1H 8M5, Canada. Tel.: 613-562-5800 (ext. 8437); Fax: 613-562-5440; E-mail: evans@uottawa.ca.

[1] The abbreviations used are: mAb, monoclonal antibody; CDR, complementarity determining region; C_{H1}, first constant region of an antibody heavy chain; C_L, constant region of an antibody light chain; DTT, dithiothreitol; ELISA, enzyme-linked immunosorbent assay; Fab, fragment comprising the antibody Fv and first constant region domain dimer; Fc, carboxyl-terminal fragment comprising the second and third

get neoplastic cells has been shown to shrink the sizes of some tumors and, in some cases, to induce regression. Successful therapy depends on many factors, such as the recognition and binding of the antibody to the tumor antigen, and the subsequent induction of an immune response leading to tumor cell death.

Research into cell-surface tumor antigens has concentrated on human melanoma malignancies, and several have been found that can induce either a humoral or cellular immune response (1, 2). Unfortunately, few antigens have been identified that are recognized by both components of the immune system. At least six humoral-mediated melanoma antigens have been reported to date, of which four have been found to be gangliosides (1, 2). Gangliosides are glycolipids consisting of a ceramide tail with an oligosaccharide head group and have long been implicated in cellular interactions, differentiation and oncogenesis (3). The ceramide moiety is sequestered within the membrane, leaving the carbohydrate moiety exposed to immune surveillance. One challenge encountered in exploiting some gangliosides as tumor antigens can be poor observed immunogenicity. This may be due, in part, to a limited presence of the ganglioside on the surface of noncancerous tissues leading to a degree of immune tolerance, and to the fact that gangliosides do not stimulate T-cell help. The low immunogenicity of some gangliosides is offset by the density with which they may be expressed on the surface of malignant cells. A further factor is the diversity of available antigens (4), where the relative abundance of many gangliosides on the cell surface changes during cancerous mutation with each different ganglioside providing a possible venue for therapy (5, 6).

One such antigen is disialoganglioside GD3, which is over-expressed on the surface of melanomas, soft tissue sarcomas, and tumors of neuroectodermal origin, while normal tissues display little or no GD3 (7). Four forms of GD3 have been identified, which vary somewhat in the substitution pattern of the terminal NANA residue (8, 9, 10). The best characterized GD3 has the structure NANA-α(2→8)-NANA-α(2→3)-Gal-β(1→4)-Glc-ceramide (Fig. 1). Several antibodies specific for this antigen have been identified, with one of the most actively investigated being the murine mAb R24. R24 has been shown to prevent tumor development in animal models (11), as well as to display anti-tumor activity in human clinical trials (12, 13, 14). One of the most intriguing aspects of R24 is its ability to

constant regions of an IgG antibody; Fv, fragment comprising the antibody variable domain dimer; Gal, galactose; GD3, disialoganglioside GD3; Glc, glucose; ID, idiotype; NANA, *N*-acetylneuraminic acid; PC, Patterson correlation; PEG, polyethylene glycol; RU, resonance unit(s); V_H, heavy chain of an antibody variable region; V_L, light chain of an antibody variable region.
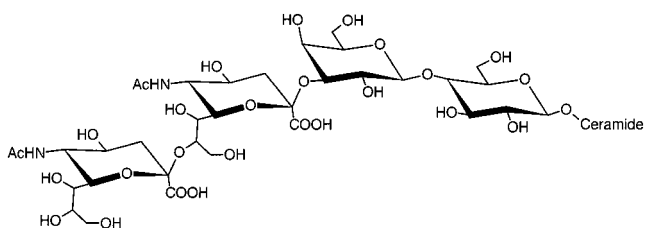
FIG. 1. **Schematic diagram of the most common form of the melanoma tumor cell antigen glycosphingolipid disialoganglioside GD3.** The ceramide tail is anchored in the cell membrane, leaving the four-sugar head group exposed to immune surveillance.

display homophilic binding through a heavy chain idiotope designated ID_{HOM} (15), where homophilic binding is the ability of an antibody to recognize and to bind itself. Homophilic binding is thought to amplify the effective valence of an antibody, and so increase its avidity. R24 has also shown the ability to bind other GD3-specific antibodies in a similar manner (16).

Interestingly, the antigen-binding site (designated by idiotope ID_{GD3}) and ID_{HOM} have been shown to be distinct, since specific mutations can disrupt homophilic binding without the loss of antigen binding (16). Homophilic binding in R24 is also distinct from the known ability of murine IgG3 to bind cooperatively to multivalent antigen through an Fc-dependent mechanism (17), because changes in residue identity in R24 near ID_{HOM} in V_H (and thus distant from the Fc) have been shown to disrupt this phenomenon (15). The avidity of a monoclonal antibody is a critical aspect of its function. Understanding the mechanism of homophilic binding in R24 will have potential impact on engineering this and other mAbs to increase their avidity without altering their specificity.

The forms of R24 that are available for study are the original murine R24 mAb, the human-murine chimer chR24, and their respective Fabs. The mAb chR24 is expressed from a construct in which the V_L and V_H murine genes have been ligated onto the human $IgG1(\kappa)$ C_L and C_H genes. This form of R24 was prepared in order to increase its effectiveness as a human therapeutic agent while maintaining its GD3-binding properties. However, preliminary surface plasmon resonance experiments indicated that the homophilic binding properties of chR24 were significantly different from those of the native R24, and a detailed comparison of the homophilic and antigen-binding behavior using several methods was therefore necessary. We present below the characterization of homophilic binding in R24 and chR24 by surface plasmon resonance and x-ray crystal structure analysis.

EXPERIMENTAL PROCEDURES

Antibody Cell Lines—Murine anti-GD3 antibody R24 $IgG3(\kappa)$ was obtained from hybridoma ascites of $(BALB/c \times C57BL)F_1$ mice (11). The mouse-human chimeric R24 (chR24) was expressed from a construct consisting of the genes coding for the R24 heavy and light variable region ligated to the respective genes coding for human $IgG1(\kappa)$ constant domains, and was provided by Dr. Alan Jarvis (Repligen Corp., Cambridge, MA).

Antibody and Fab Generation and Purification—R24 and chR24 antibodies were purified from ascites using Protein A affinity column chromatography (Bio-Rad). Although ascites does contain immunoglobulins other than R24 or chR24 that will bind to a Protein A affinity column, the purity of the mAb preparations was evident by inspection of isoelectric focussing gels and by the subsequent crystallization of the antigen-binding fragments. Fab fragments were prepared from the purified antibodies by digestion with mercuripapain (Sigma, P-9886). Mercuripapain was activated by β-mercaptoethanol as described previously (18). The mAb digest mixture contained IgG:papain in a 200:1 (w/w) ratio, and carried out in the presence of DTT (8:1 DTT:IgG molar ratio) and brought to final volume with 20 mM sodium acetate, pH 5.4. The digest reactions were quenched with iodoacetamide equivalent to 2.2 mol of DTT. Time trial results established optimal digests at 3.5 h

for R24 and 2.5 h for chR24. Quenched digest mixture was dialyzed overnight against 20 mM sodium acetate, pH 5.4. The dialyzed digest was then filtered on a 0.22-μm low protein-binding filter, and degassed in preparation for high performance liquid chromatography purification (Gilson series 800 HPLC system, Gilson Scientific Canada, Inc.). The Fab fragments were applied to a Shodex IEC-CM825 ion exchange column (Phenomenex) in a mobile phase of 20 mM sodium acetate, pH 5.4, and eluted against a 0–2 M sodium chloride gradient. Protein content was assayed by absorption at 280 nm wavelength; $A_{280}/1.5$ was used to calculate the Fab concentration (in mg/ml). Absorbing fractions were assayed by SDS-polyacrylamide gel electrophoresis (Pharmacia Phast System, 12.5% homogeneous gels), to identify the fractions containing Fab, which were pooled and concentrated (Centricon-10, Amicon) to between 8 and 12 mg/ml. Sodium azide was added to the concentrated Fab at 0.02% (w/v). The concentrated Fabs were kept at 4 °C prior to crystallization trials.

Crystallization—Primary determination of crystallization conditions for the Fabs from both R24 and chR24 were carried out using Crystal Screen I and II (Hampton Research, Laguna Hills, CA). Screens were carried out by mixing 1 μl of concentrated Fab with 1 μl of reservoir buffer and the resultant drop suspended on a plastic coverslip over 1 ml of reservoir buffer in a Linbro tissue culture 24-well plate (ICN Biomedicals, Inc., Aurora, OH). Refinement conditions were generated using reagents from Fluka Biochemika.

X-ray Crystal Structure Analysis—Data collection was carried out at Queens University (Kingston, Ontario, Canada) using a MAR 30-cm image plate mounted on an Rigaku RU-II generator running at 6 kilowatts. Data reduction was carried out using DENZO (19). Rotation functions were carried out with MERLOT (20). Translation functions and positional refinements were carried out with XPLOR (21). Molecular modeling and fitting of electron density were carried out with FRODO (22) and SETOR (23). All molecular and electron density diagrams were generated using SETOR and SETORPLOT (23).

Surface Plasmon Resonance—Analyses were performed using a BIACORE 1000 biosensor system (Biacore Inc., Piscataway, NJ). Fabs used in the experiments were from the same lot used for crystallization studies. For antigen binding studies, ganglioside GD3 (BioCarb Chemicals) was incorporated into liposomes also containing dimyristoylphosphatidylcholine and *Salmonella* serogroup B lipopolysaccharide as described previously (24). Se155-4, an IgG specific for the *Salmonella* antigen, was immobilized on research grade CM5 sensor chips (Biacore Inc.) and served as a capture molecule for the GD3 liposomes (24). Liposomes (1000 RU) were captured followed by injection of murine R24 IgG, chR24 IgG, murine R24 Fab, or chR24 Fab over the liposome surfaces. IgG concentrations were calculated on a per binding site basis. The liposome experiments were carried out in 10 mM HEPES, pH 7.4, 150 mM sodium chloride, 3.4 mM EDTA. Control surfaces were prepared in the same way by capturing liposomes containing only dimyristoylphosphatidylcholine and lipopolysaccharide. The Se155-4 IgG surfaces were regenerated by sequential injection of 1 and 4 mM sodium taurodeoxycholate in 10 mM sodium acetate buffer, pH 4.5, and a contact time of 3 s in each instance. For the measurement of homophilic binding under solution-like conditions, murine R24 IgG was immobilized on research grade CM5 sensor chips using the amine coupling kit supplied by the instrument manufacturer. Mouse R24 IgG was then injected over this surface using the phosphate-buffered saline, 0.05% Tween 20, 1% bovine serum albumin, pH 7.4, buffer employed in Ref. 15 for the measurement of homophilic binding by ELISA. Primary sensorgram data were evaluated using the BIAevaluation 3.0 software.

RESULTS

Crystallization of the Fab from R24—Small crystals were noted for Crystal Screen I solutions 33, 36, and 45, and the drop sizes were scaled up to 4 and 6 μl and refinements proceeded by varying the pH of the solution along with the concentration and composition of precipitants. Solution 33 (originally 4.0 M sodium formate) yielded crystals after a few weeks with an average size of $0.1 \times 0.25 \times 0.2$ mm^3 from a solution at pH 7.5. Solution 36 (originally 8% PEG 8000, Tris-HCl, pH 8.5) yielded crystals in a few days with an average size of $0.15 \times 0.2 \times 0.3$ mm^3 from both 8% PEG 8000 in Tris-HCl at pH 8.0 and at pH 8.5, and from 10% PEG 8000 in Tris-HCl at pH 8.0. Solution 45 (originally 18% PEG 8000, 0.1 M sodium cacodylate, pH 6.5, 0.2 M zinc acetate) yielded crystals with an average size of $0.2 \times 0.2 \times 0.25$ mm^3 from this solution and from 23% PEG 8000, 0.2

M zinc acetate in 0.1 M sodium cacodylate, pH 7.0, from which grew the crystal that gave the highest resolution data.

Crystallization of the Fab from chR24—Solution 45 from Crystal Screen I (0.2 M zinc acetate, 0.1 M sodium cacodylate, pH 6.5, 18% PEG 8000) yielded small crystals after 1 week. Initial refinements were carried out at 4 °C and 20 °C, and consisted of combinations of pH from 6 to 8.5 in increments of 0.5, PEG 4000, 8000, and 10,000, at concentrations of 13, 18, and 23%, with the concentrations of zinc acetate and sodium cacodylate kept constant. The crystal selected for data collection was obtained by macroseeding a drop of 0.2 M zinc acetate and 0.1 M sodium cacodylate at pH 7.0 with 23% PEG 8000.

X-ray Diffraction Data Collection—For crystals of the Fab from R24, 58,762 reflections were measured yielding 26,595 unique reflections to 3.1-Å resolution (92% complete) with R_{sym} = 0.075. The Fab was found to crystallize in the monoclinic space group $P2_1$ with cell dimensions a = 139.2, b = 82.1, c = 73.6 Å, and β = 94.1°. For crystals of the Fab from chR24, 79,380 reflections were measured yielding 18,143 unique reflections to 2.5-Å resolution (94% complete) with R_{sym} = 0.050. The protein was found to crystallize in the monoclinic space group $C2$ with cell dimensions a = 146.8, b = 56.0, c = 80.0 Å, and β = 119.2°.

Structure Solution—The structure of the Fab from murine R24 was solved by molecular replacement methods using the known structure of the Fab from YsT9.1 specific to *Brucella abortus* as a trial structure (25, 26). The volume of the unit cell indicated that it probably contained three molecules of R24 Fab per asymmetric unit; however, the rotation solution revealed at best only two clear solutions for the model of the constant domain dimer no matter what combination of resolution range, σ cutoff, and integration radius was used. The best results were found using all data with an input resolution range of 6 to 4 Å and integration radius of 23 Å. The translation solution for the two fragments (including the cross-translation function) was determined with the aid of the Patterson correlation (PC) refinement function in XPLOR. The two variable domain dimers were positioned by executing individual elbow-angle searches using PC refinement about the corresponding constant domain dimers. Several rounds of rigid-body refinement with all data from 6 to 4 Å resolution with $I \geq 3(\sigma)I$ were carried out using first the entire Fab as a rigid body, then the intact variable and constant domains, and finally the heavy and light chains of each of the two domains. This resulted in an R-factor of 0.26. The sequence corresponding to R24 was then imposed on the model using SETOR. Hendrickson-Konnert refinements were carried out, alternating with rounds of manual intervention to position the CDRs and other residues. Due to the limited resolution of the data (3.1 Å), all data (*i.e.* no σ cutoff) was used for the final cycles of refinement, no water molecules were added to the trial structure, and individual temperature factors were not allowed to refine independently. As the nature of the interaction between the two molecules in the asymmetric unit was the object of the analysis, the observed non-crystallographic two-fold symmetry axis was not applied during refinement. The R-factor converged at 0.245 for all data. The final refined overall isotropic temperature factor was 28.4 Å^2, which is somewhat lower than the value of 35.3 Å^2 obtained from a Wilson plot. An R_{free} was calculated in a separate refinement to be 0.334, which indicated that the refined model was somewhat underdetermined at 3.1-Å resolution.

The structure of the Fab from chR24 was determined using the structure for R24 as a trial structure. A search using XPLOR clearly revealed the orientation and position of the variable domain dimer of chR24 (which has the same sequence as the corresponding domain dimer from R24). An elbow-angle search combined with PC refinement in XPLOR revealed the position of the constant domain dimer. The sequence of the constant domains of both the heavy and light chains were changed to correspond to human IgG1(κ) using SETOR. Refinement proceeded as for R24; however, there were enough data for individual isotropic temperature factors to be refined and for the positions of several water molecules to be assigned. The structure was refined to a final resolution of 2.5 Å, with a final R-factor of 0.162 for all data with $I \geq 2\sigma(i)$, with 74 water molecules.

Quality of the X-ray Crystal Structures—The standard deviation of the distribution of the bond lengths and bond angles about ideal values after the final cycles of refinement was found to be 0.022 Å and 3.8°, and 0.015 Å and 1.35° for R24 and chR24, respectively. The Ramachandran plots (not shown) for both structures reveal that few non-glycine residues lie outside the allowed regions. The electron density is well defined over the course of most of the polypeptide chain, even for the 3.1 Å resolution R24 structure. Interestingly, it was the lower resolution R24 structure that was solved first, where the trial phases from the molecular replacement solution were sufficient to trace the entire polypeptide chain. The conformations of all six CDRs in both structures lie in well defined electron density, and the H2 CDR loops from both structures are presented in Fig. 2.

Comparison of R24 and chR24 Structures—The positions of all atoms in the two molecules in the asymmetric unit for R24 were refined independently. Although the R24 Fab crystals scattered to only 3.1 Å resolution, a least-squares superposition of the α-carbon atoms applied separately to the Fv and C_{H1}-C_L domain dimers of the two molecules shows no significant difference in the positions of main chain atoms, and small changes in conformation of a few side chains. The "elbow" angles (defined as the angle subtended by the pseudo two-fold axes of the variable and constant domains of an Fab) are not significantly different between R24 and chR24 at 166.7 and 167.3°. A least-squares superposition of the α-carbon atoms of the Fvs of chR24 onto either Fv from R24 gives a root-mean-square deviation of less than 1.0 Å, and shows that the humanization process has had no significant effect on the conformation of the Fv.

Characterization of Homophilic Binding—Surface plasmon resonance experiments showed that both murine R24 IgG and chimeric chR24 IgG bound to GD3-bearing liposome surfaces, but with strikingly different affinities (Fig. 3, *a* and *b*). At concentrations of 2 μM, R24 gave a response of 1700 RU at the end of the injection whereas chimeric R24 IgG gave a response of only 35 RU under the same conditions. The most interesting feature of the sensorgrams is the apparent lack of saturation associated with R24 binding to GD3-bearing liposomes. This is characteristic of homophilic binding, and is similar to the results reported previously for the binding of R24 IgG to human melanoma cell lines expressing GD3 (15). The binding kinetics were observed to be complex at all concentrations of IgG. Distinctly biphasic behavior was evident at higher R24 IgG concentrations of 1 and 2 μM. A "fast-binding" phase is observed to dominate in the first few seconds, accounting for approximately 70% of the bound antibody, followed by a "slow-binding" phase, which gradually increases the amount of bound antibody over a period of several minutes. The rapid initial association may reflect both GD3 antibody recognition and homophilic binding, with the slower association attributable solely to homophilic interactions. The kinetics are simpler at lower concentrations of R24 (Fig. 3*a*, *inset*) where biphasic behavior is not observed; however, even these data do not fit to a simple bivalent analyte model. The data collected at lower IgG concentrations do fit
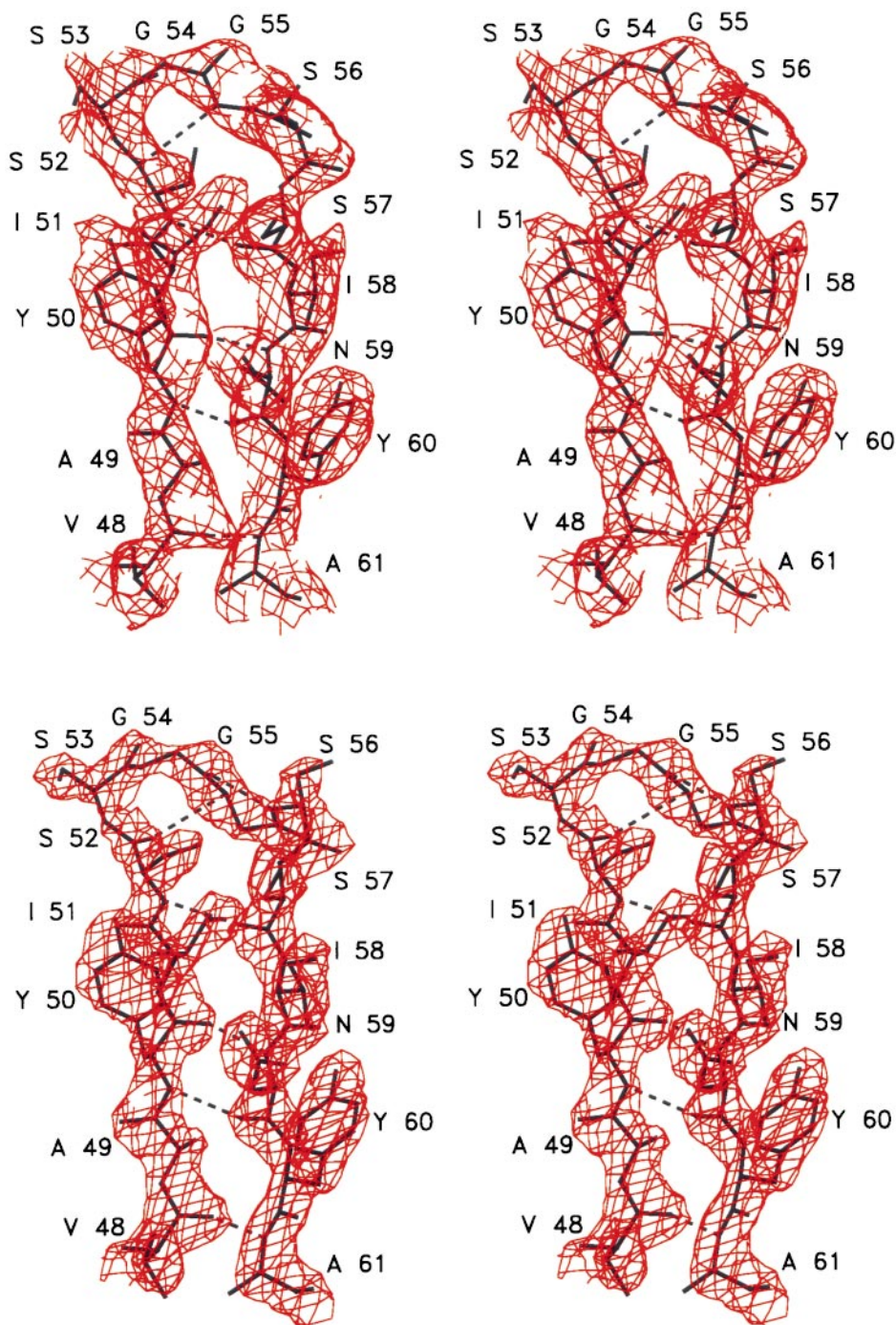
FIG. 2. **Stereoview of the wireframe models (*solid black lines*) and corresponding observed electron density (*red lines*) for the H2 hypervariable loop for the R24 (*top*) and chR24 (*bottom*) Fabs, contoured at 1.5 and 2.0 σ, respectively.** Observed hydrogen bonds are shown as *dashed black lines*. The electron density for the R24 structure is exceptional, given that the data extend to 3.1-Å resolution.

well to a simple one-to-one interaction model, which gives an association rate constant of 1.3×10^5 M^{-1} s^{-1} and a dissociation rate constant of 2.3×10^{-3} s^{-1} ($K_D = 18$ nM). It was not possible to derive similar rate constants for chR24 because complex biphasic binding is observed at all concentrations (Fig. 3b).

Scatchard analysis of equilibrium binding data obtained for the binding of murine R24 Fab to liposomes containing 10% GD3 is presented in Fig. 4. The plot of bound *versus* bound/free R24 shows that homophilic binding was occurring, as a straight line with a positive slope indicates that the proportion of available Fab that bound to liposomes increases with increasing Fab concentration. The extent of Fab dimerization resulting from homophilic binding would increase with concentration, and the resulting higher proportion of bivalent Fab would be manifested as increased functional affinity. Equilibrium binding

was achieved very rapidly at the Fab concentrations used, and the dissociation of Fab from the liposomes was too rapid to allow the derivation of kinetic constants. These results also agree with reported experiments binding R24 IgG to human melanoma cell lines (15). Scatchard analysis of the R24 IgG data did not give a straight line and confirmed the non-saturable nature of analyte binding. It is not surprising that the IgG data was not as easily analyzed as that of the Fab, since bivalency adds complexity to the binding reaction.

The affinity of chR24 Fab for GD3-bearing liposomes was significantly weaker than that of the murine Fab. A concentration of 80 μM gave an equilibrium response of 160 RU; this is the same response obtained with murine R24 at a concentration of 6 μM. A Scatchard plot of the equilibrium binding data obtained with chR24 Fab was consistent with non-saturable binding in that a line with a slope of zero was obtained instead
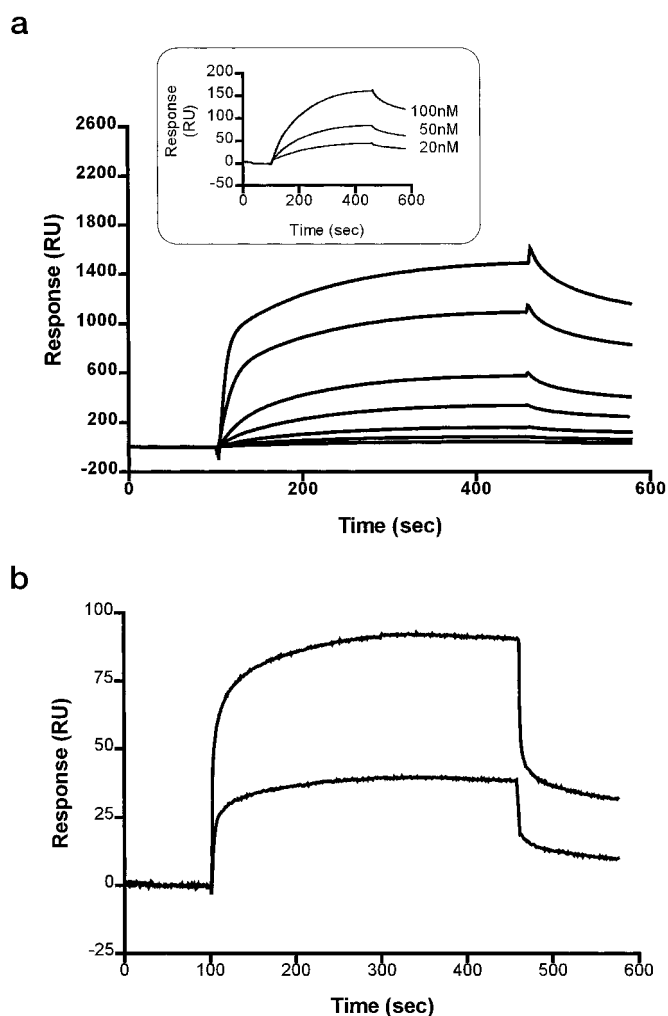
a

b

FIG. 3. **BIACORE sensorgrams showing the binding of R24 IgGs to GD3 liposomes.** *a*, murine R24 IgG at concentrations of 20, 50, 100, 200, 500, 1000, and 2000 nM. The *inset* shows an expanded *y* axis for the lowest three concentrations. *b*, chimeric chR24 at concentrations of 2 and 5 μM.
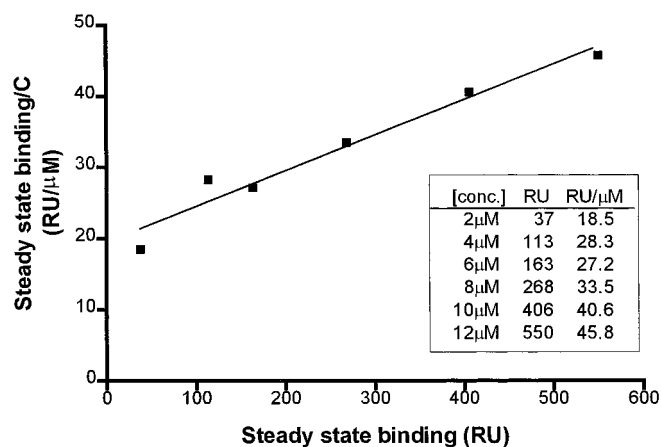

[conc.]	RU	RU/μM
2μM	37	18.5
4μM	113	28.3
6μM	163	27.2
8μM	268	33.5
10μM	406	40.6
12μM	550	45.8

FIG. 4. **Scatchard plot of equilibrium binding data for murine R24 Fab binding to liposomes containing 10% GD3.** The equilibrium responses, after control surface subtraction, at different Fab concentrations are given in the *inset*.

of the negative slope expected for a simple one-to-one interaction.

By SPR analysis, R24 homophilic binding was only observed in the presence of GD3-bearing liposomes. When R24 IgG was covalently coupled to the dextran matrix of the sensor chips to give IgG surface densities of 12,500 RU, which corresponds to approximately 12.5 ng/mm^2, injected R24 IgG at concentrations as high as 1 μM, did not bind to these surfaces, showing that no significant level of homophilic binding occurs in the absence of liposomes containing GD3. This is in contrast to ELISA data, which showed significant binding of biotinylated R24 IgG, over a concentration of 1–100 μg/ml (0.01–1.3 μM), to plates coated with R24 IgG at a concentration of 5 μg/ml (15). Coating the ELISA plate at this antibody concentration would give an IgG surface density of 3 ng/mm^2 if 100% of the antibody adsorbed to the plate. The discrepancy between the ELISA data and the SPR results obtained using immobilized IgG may reflect the fact that IgG would exist under solution-like conditions when linked to dextran chains on sensor chips, whereas adsorption to microtiter plates would present the IgG in a rigid two-dimensional environment more closely resembling cell membrane and liposome surfaces.

DISCUSSION

Comparison of the Fabs from R24 and chR24—The chR24 mAb is a chimer, with the Fv domain sharing sequence identity with the Fv from R24, and with the C_{H1}-C_L domain dimer corresponding to human IgG1(κ). The chR24 mAb was created in order to preserve the GD3 recognition site while lowering in humans the degree of adverse immune reaction against a murine mAb. This is the first report of the three-dimensional structures of both the uncomplexed murine Fab and mouse-human Fv- C_{H1}-C_L chimer. The two published reports of chimeric Fab structures describe, respectively, the structure of a native murine Fab (27), and a comparison of the complexed and uncomplexed forms of a chimeric Fab (28). The interface between the Fv and C_{H1}-C_L domain dimers has been implicated in transmitting an allosteric response to binding from the Fv to the C_{H1}-C_L domain dimer of the Fab upon complexation with antigen (29). The transition from murine to human amino acids occurs after residues Leu-108 and His-123, which are both located in hinge regions of the Fab. The elbow angle for chR24 is comparable to R24, and the constant domains of chR24 occupy a position and orientation that is close to the native murine form.

GD3 Binding Site—R24 and chR24 antibodies are specific for the ganglioside GD3 (8, 9, 10), of which the most common form consists of NANA-α(2→8)-NANA-α(2→3)-Gal-β(1→4)-Glc-ceramide (Fig. 1). Examination of the binding surface of the Fvs shows that the three CDRs of the V_H cooperate to form a deep pocket which serves to recognize and to bind the antigen (Fig. 5). The pocket is lined by polar amino acids (serine, threonine, histidine) as well as some tyrosine residues and has a well defined mouth or lip. The pocket measures approximately 8.5 × 12 × 8 Å^3, which allows it to completely accommodate the terminal sialic acid residue on GD3. The substitution of the C_L-C_{H1} domains has had little effect on the conformation of residues lining the binding pocket between the R24 and chR24 structures, as a superposition of the residues lining the binding pocket of chR24 shows a root-mean-square deviation of only 0.56 Å.

Characterization of Homophilic Binding—The binding to liposomal GD3 of R24 and chR24 IgG and Fab was investigated in order to better understand the factors contributing to their different binding profiles, especially given that mutations in V_H have been shown to disrupt the homophilic binding phenomenon in chR24 (16). Murine R24 IgG displays strong binding to GD3-bearing liposomes, which can be attributed to homophilic binding between molecules of R24 and the formation of a multivalent antibody lattice. The reduced levels of binding displayed by the chimeric chR24 IgG reveal the heavy participation of the constant regions of the murine R24 IgG in ho-

FIG. 5. **Stereoview of the surface (*red*) of the heavy chain of chR24 showing the α-carbon backbone of the three CDR loops (*black*).** The pocket formed by H1, H2, and H3 is large enough to accommodate the terminal sialic acid residue of ganglioside GD3.
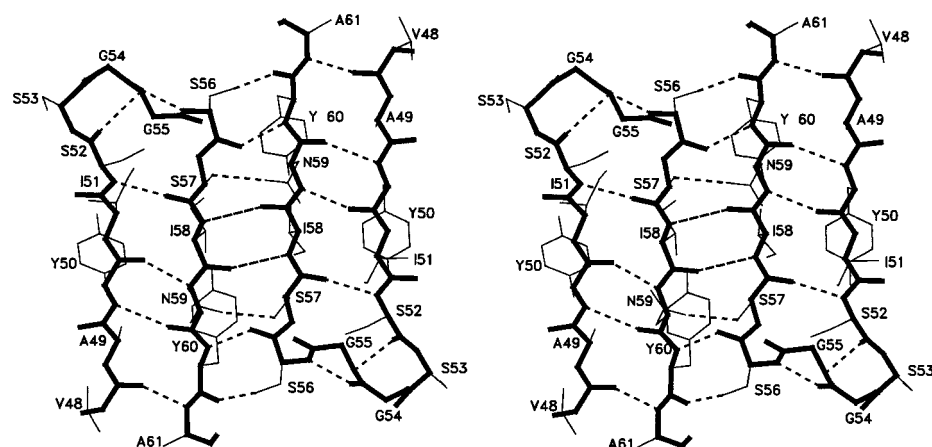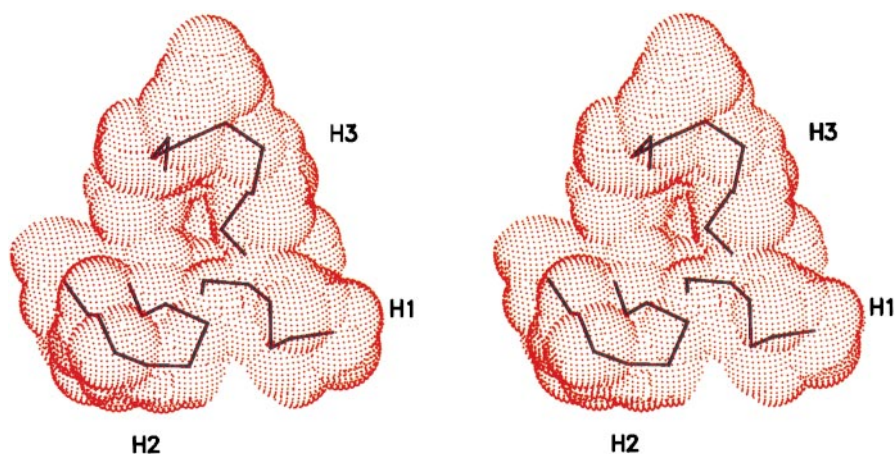

FIG. 6. **Stereoview of the wire frame model of the area of dimerization between the H2 loops of two molecules of chR24 in the crystal lattice, with the positions of main chain (*thick*) and side chain (*thin*) atoms as well as observed hydrogen bonds (*dashed*).** Amino acids are labeled with their residue *number* and corresponding *single-letter codes*. The interactions are similar to those observed in the R24 dimer.

mophilic binding. As the structures of the Fvs of R24 and chR24 have been found in this study not to be significantly different, the difference in activity observed between R24 and chR24 must stem from the change in constant regions from murine IgG3(κ) to human IgG1(κ). Similar differences in antibody affinities that accompany changes in constant region subclass have been reported (30), and attributed largely to the ability of murine IgG3 antibodies to form multivalent lattices. However, the chimeric chR24 antibody with its human IgG1 heavy chain still displays some homophilic binding.

Loss of homophilic binding in chR24 had been demonstrated previously to occur in certain V_H mutants, leading to the assignment of a specific idiotope for homophilic binding designated ID_{HOM} (16). The levels of homophilic binding that are displayed by chR24 IgG can be attributed directly to cooperative V_H-V_H interactions through ID_{HOM}.

Interestingly, neither the R24 or chR24 IgGs display a significant level of homophilic binding under solution conditions, indicating that there is a requirement for the GD3 antigen and/or a membrane-like surface to induce this phenomenon. Thus, stable binding of GD3 by R24 is a cooperative process requiring V_H-V_H interactions (which can be disrupted by single point mutations), Fc-Fc interactions (apparent from the difference between R24 Fab and IgG binding), and the immobilized antigen presented on a membrane. The formation of antibody lattices on cell surfaces would obviously also be influenced by GD3 concentration in the membrane.

A significant difference in binding was also observed between the R24 and chR24 Fabs, where the Fab from R24 again showed superior homophilic binding ability. Like their parent molecule, the Fabs from murine IgG3 antibodies display the ability to form multivalent species through their constant regions. This behavior of murine R24 manifested itself during crystallization trials, where the protein was found to be less soluble than the Fab from chR24 (2.5 *versus* 12 mg/ml).

Fab Dimerization and the Assignment of ID_{HOM}—Structural studies of the Fabs corresponding to R24 and chR24 were undertaken to allow a characterization of the interactions of the variable domains in the crystalline state in the absence of the Fc. The Fabs from both R24 and chR24 are indeed observed to form dimers in the crystal lattice. R24 crystallizes in space group $P2_1$, where the dimers are composed of two independent molecules in the asymmetric unit related by a non-crystallographic two-fold axis of symmetry. Fabs corresponding to chR24 crystallize in space group $C2$, where the dimers are composed of two molecules related by a true crystallographic two-fold axis. Despite the difference in packing arrangement, the dimerization interactions exhibited by R24 and chR24 are almost identical. A schematic and wire-frame model of the

TABLE I
Interactions formed along the homophilic dimer interface of R24 and chR24

Main-chain hydrogen bonds				
Ser	H56	O . . . H-N	Tyr	H60
Ile	H58	N-H . . . O	Ile	H58
Ile	H58	O . . . H-N	Ile	H58
Tyr	H60	N-H . . . O	Ser	H56
Side-chain hydrogen bonds				
Ser	H56	OH . . . O	Tyr	H60
Ser	H57	OH . . . H-ND	Asn	H59
Asn	H59	ND-H . . . OH	Ser	H57
Tyr	H60	O . . . OH	Ser	H56
Hydrophobic interactions				
Ile	H58	. . .	Ile	H58

contact area of dimerization for chR24 in the solid state is given in Fig. 6. The dimerization proceeds though a continuation of the anti-parallel β-sheet structure of the H2 loop. Table I details the four observed intermolecular main chain hydrogen bonds that are formed, and lists several side chain hydrogen bonds and a hydrophobic interaction that contribute to the stability of the dimer. The dimer displays a degree of flexibility in that R24 and chR24 display slightly different dimerization geometry. The angles between the pseudo two-fold axis of the V_L and V_H are 167° in R24 and 155° in chR24. Examination of the rotational freedom about the β-sheet interface shows that the dimer can flex through an angle of approximately 20° without generating significant steric interactions, or disrupting the intermolecular β-sheet interaction.

The remaining intermolecular contacts made by the Fab dimers in the crystal lattice are different in R24 and chR24, where R24 shows contacts from all various of heavy and light chains, while chR24 displays contacts primarily from the V_L domains to the C_{H1} domains of neighboring Fabs in the crystal lattice.
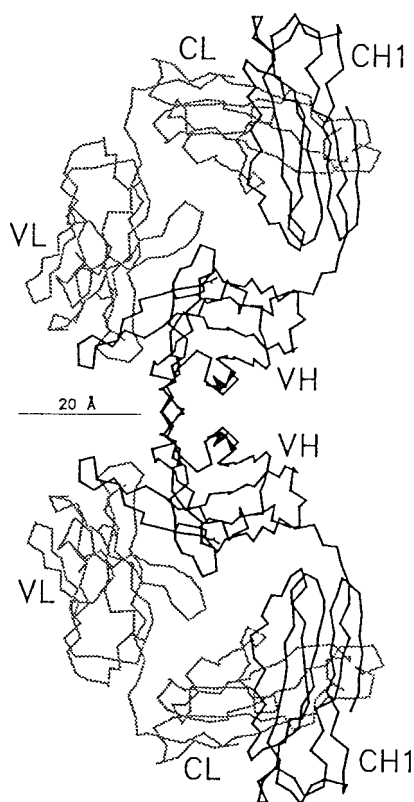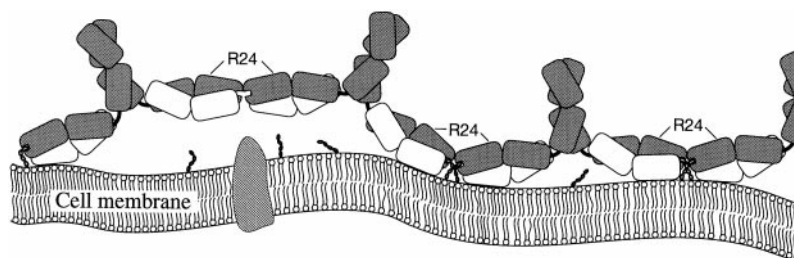

FIG. 7. **View of the α-carbon backbone of chR24 dimer showing the relative positions of the light (*gray lines*) and heavy (*black lines*) chains.** A distance of 20 Å is also indicated. The pocket that can recognize and bind to the terminal NANA residue on GD3 lies approximately 18 Å from the "left" edge of the Fab, which is an appropriate distance in order to bind membrane-anchored antigen.

FIG. 8. **Model of the formation of an chR24 mAb lattice on the membrane of transformed cells expressing large amounts of ganglioside GD3.** Molecules of R24 or chR24 are able to simultaneously bind GD3 antigen, other molecules of R24, and interact with the membrane surface through the variable domain of the light chain. The large number of cooperative interactions stabilize the formation of an R24 lattice on the cell surface, which increases the effective valence of the antibody.

Fab Dimerization and the Formation of an Antibody Network—An α-carbon backbone of the chR24 dimer as it occurs in the crystal structure is presented in Fig. 7. The orientation of the two-fold axis relating the Fvs is such that the N terminus of the heavy chains of the two Fabs in the dimer can approach the cell surface close enough to simultaneously bind the terminal residue of GD3 in the antigen-binding pocket while in the dimerized state.

This conformation of the dimer in combination with the surface plasmon resonance studies leads to a model for the formation of an antibody network. Fig. 8 depicts a tumor cell expressing ganglioside GD3 on its surface and the resulting antibody network in which molecules of chR24 are bound to the surface antigen and to each other through ID_{HOM}. The necessary proximity of the dimer Fv surfaces to the membrane serves to immobilize and stabilize the dimer, and allows for possible interactions between the membrane and the Fv. This model explains the apparent requirement for the presence of the membrane, and why R24 is a relatively labile dimer in solution but forms strong homophilic networks while bound to a GD3-bearing surface. The large number of cooperative interactions formed by the mAb lead to stabilization of the dimer and to the formation of larger antibody networks. The cooperative network of dimers would give the antibody a high potential valence, leading to a low off rate.

Comparison with Reported Structures of Antibody Antigen-binding Sites—Of the Fab and Fv structures deposited in the Protein Data Bank (31) that were accessible to date, only one other structure (the Fab from mAb HIL; code 8FAB) displays dimerization through any part of the Fv site. The dimerization of HIL occurs though a similar pairing of the H2 loop main chain and side chain interactions as found for R24 and chR24. Four major canonical conformation have been associated with the H2 loop (32), which are represented schematically in Fig. 9. R24, chR24, and HIL all have H2 loops that belong to type 3, which is the only conformation in which all the main chain
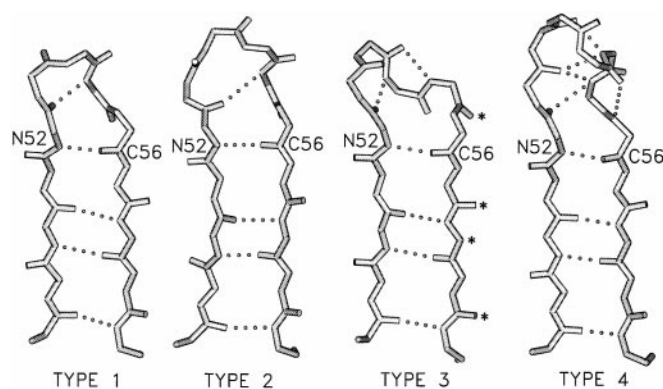

FIG. 9. **Schematic representations of the four canonical conformations for the H2 loops observed in ref 32.** Only type 3 loops have all main chain hydrogen bonding groups oriented to form β-sheet dimerization (shown by *asterisks*). The R24 and chR24 structures are characteristic of type 3 H2 loops.

hydrogen bonding groups are positioned to form an anti-parallel β-sheet interaction. The formation of main chain hydrogen-bonded pairs in the crystal lattice has not been observed for type 1, 2, and 4 H2 loops.

There are at least 12 other Fab or Fv structures that display type 3 H2 loop conformations, yet only R24 chR24 and HIL display dimerization through the H2 loop. This indicates that not only must the H2 canonical form be present on the Fab, it must also possess a primary structure that is capable of forming appropriate side chain interactions. Evidence for this point can be seen in studies of homophilic binding for chR24 mutants (16), where changes in residue identity at or near ID_{HOM} almost always disrupt homophilic binding.

Interestingly, β-sheet dimerization of Fabs is not restricted to the Fv. Three other structures (7FAB (33), 1DBJ (34), 1GGB (35)) show β-sheet coupling through their C_{H1} domains, and well away from the antigen-binding site. The parent antibodies of these three structures do not share a common heavy chain, being, respectively, murine IgG1, murine IgG2a, and human IgG1. Homophilic binding through the first constant region can serve a purpose similar to binding through the Fv, but cannot be properly classed as an idiotope.

Significance of Homophilic Binding in Cancer Therapy— Direct comparisons in mouse models of the therapeutic value of high and low affinity mAbs suggest that higher affinity antibodies are more effective in cancer treatment (36, 37). The changes observed in R24 and chR24 antigen binding that occur with the changes in their ability to display homophilic binding demonstrate that this class of phenomenon should be explored further as a means of increasing effective antigen affinity without altering specificity.

REFERENCES

1. Lloyd, K. O. (1993) in *Specific Immunotherapy of Cancer with Vaccines* (Bystryn, J.-C., Ferrone, S. & Livingston, P., eds) pp. 50–58, New York Academy of Sciences, New York
2. Boon, T. (1993) *Int. J. Cancer* **54,** 177–180
3. Hakamori, S. (1981) *Annu. Rev. Biochem.* **50,** 733–764
4. Irie, R. F. & Ravindranath, M. H. (1990) in *Therapeutic Monoclonal Antibodies* (Borrebaeck, C. A. K. & Larrick, J. W., eds) pp. 75–85, Stockton Press, New York
5. Albino, A. P., Houghton, A. N., Eisinger, M., Lee, J. S., Kantor, R. R., Oliff, A. I. & Old, L. J. (1986) *J. Exp. Med.* **164,** 1710–1722
6. Carubia, J. M., Yu, R. K., Macala, L. J., Kirkwood, J. M. & Varga, J. M. (1984) *Biochem. Biophys. Res. Commun.* **120,** 500–504
7. Hamilton, W. B., Helling, F., Boon, K. O. & Livingston, P. O. (1993) *Int. J. Cancer* **53,** 566–573
8. Pukel, C. S., Lloyd, K. O., Travassos, L. R., Dippold, W. G., Oettgen, H. F. & Old, L. J. (1982) *J. Exp. Med.* **155,** 1133–1147
9. Thurin, J., Herlyn, M., Hindsgaul, O., Stromberg, N., Karlsson, K. A., Elder, D., Steplewski, Z. & Koprowski, H. (1985) *J. Biol. Chem.* **260,** 14556–14563
10. Hirabayashi, Y., Higashi, H., Kato, S., Taniguchi, M. & Matsumoto, M. (1987) *Jpn. J. Cancer Res.* **78,** 614–620
11. Chapman, P. B., Longberg, M. & Houghton, A. N. (1990) *Cancer Res.* **50,** 1503–1509
12. Vadhan-Raj, S., Cordon-Cardo, C., Carswell, E. A., Mintzer, D., Dantis, L., Duteau, C., Templeton, M. A., Oettgen, H. F., Old, L. J. & Houghton, A. N. (1988) *J. Clin. Oncol.* **6,** 1636–1648
13. Caulfield, M. J., Barna, B., Murthy, S., Tubbs, R., Sergi, J., Mendendorp, S. &. Bukowski, R. M. (1990) *J. Biol. Response Modif.* **9,** 319–328
14. Raymond, J., Kirkwood, J., Vlock, D., Rabkin, M., Day, R., Whiteside, T., Herberman, R., Mascari, R. & Simon, B. (1991) *Proc. Am. Soc. Clin. Oncol.* **10,** 298 (abstr.)
15. Chapman, P. B., Yuasa, H. & Houghton, A. N. (1990) *J. Immunol.* **145,** 891–898
16. Yan X., Evans, S. V., Kaminski, M. J., Gillies, S. D., Reisfeld, R. A., Houghton, A. N. & Chapman, P. B. (1996) *J. Immunol.* **157,** 1582–1588
17. Greenspan, N. S., Monafo, W. J. & Davie, J. M. (1987) *J. Immunol.* **138,** 285–292
18. Yamaguchi, Y., Kim, H., Kato, K., Masuda, K., Shimada, I. & Arata, Y. (1994) *J. Immunol. Methods* **181,** 259–267
19. Otwinowski, Z & Minor, W. (1996) *Methods Enzymol.* **276,** 307–326
20. Fitzgerald, P. M. D. (1988) *J. Appl. Crystallogr.* **21,** 273–278
21. Brünger, A. T. (1992) *X-PLOR Manual*, Version 3.0, Yale University Press, New Haven, CT
22. Jones, T. A. (1978) *J. Appl. Crystallogr.* **11,** 268–272
23. Evans, S. V. (1993) *J. Mol. Graphics* **11,** 134–138
24. MacKenzie, C. R., Hirama, T., Lee, K. K., Altman, E. & Young, N. M. (1997) *J. Biol. Chem.* **272,** 5533–5538
25. Rose, D. R., Przybylska, M., To, R. J., Kayden, C. S., Oomen, R. P., Vorberg, E., Young, N. M. & Bundle, D. R. (1993) *Protein Sci.* **2,** 1106–1113
26. Evans, S. V., Rose, D. R., To, R., Young, N. M. & Bundle, D. R. (1994) *J. Mol. Biol.* **241,** 691–705
27. Brady, R. L., Edwards, D. J., Hubbard, R. E., Jiang, J.-S., Lange, G., Roberts, S. M., Todd, R. J., Adair, J. R., Emtage, J. S., King, D. J. & Low, D. C. (1992) *J. Mol. Biol.* **227,** 253–264
28. Sheriff, S., Chang, C.-Y. Y., Jeffrey, P. D. & Bajorath, J. (1996) *J. Mol. Biol.* **259,** 938–946
29. Guddat, L. W., Shan, L., Anchin, J. M., Linthicum, D. S. & Edmundson, A. B. (1994) *J. Mol. Biol.* **236,** 247–274
30. Cooper, L. J. N., Robertson, D., Granzow, R. & Greenspan, N. S. (1994) *Mol. Immunol.* **31,** 577–584
31. Bernstein, F. C., Koetzle, T. F., Williams, G. J., Meyer, E. F., Jr., Brice, M. D., Rodgers, J. R., Kennard, O., Shimanouchi, T & Tasumi, M. (1977) *J. Mol. Biol.* **112,** 535–542
32. Chothia, C., Lesk, A. M., Tramontano, A., Levitt, M., Smith-Gill, S. J., Air, G., Sheriff, S., Padlan, E. A., Davies, D., Tulip, W. R., Colman, P. M., Spinelli, S., Alzari, P. M. & Poljak, R. J. (1989) *Nature* **342,** 877–883
33. Saul, F. & Poljak, R. J. (1992) *Proteins* **14,** 363–371
34. Arevalo, J. H., Taussig, M. J. & Wilson, I. A. (1994) *Nature* **365,** 859–863
35. Stanfield, R. L. Takimoto-Kamimura, M., Rini, J. M., Profy, A. T. & Wilson, I. A. (1993) *Structure* **1,** 83–93
36. Kievit, E., Pinedo, H. M., Schluper, H. M., Haisma, H. J. & Boven, E. (1996) *Br. J. Cancer* **7,** 457–464
37. Velders, M. P., van Rhijn, C. M., Briaire, I. H., Fleuren, G. J., Warnaar, S. O. & Litvinov, S. V. (1995) *Cancer Res.* **55,** 4398–4403

The Role of Homophilic Binding in Anti-tumor Antibody R24 Recognition of Molecular Surfaces: DEMONSTRATION OF AN INTERMOLECULAR β-SHEET INTERACTION BETWEEN VH DOMAINS

Marcin J. Kaminski, C. Roger MacKenzie, Marilyn J. Mooibroek, Tanya E. S. Dahms, Tomoko Hirama, Alan N. Houghton, Paul B. Chapman and Stephen V. Evans

Access the most updated version of this article at http://www.jbc.org/content/274/9/5597

Alerts:
- When this article is cited
- When a correction for this article is posted

Click here to choose from all of JBC's e-mail alerts

This article cites 34 references, 10 of which can be accessed free at
http://www.jbc.org/content/274/9/5597.full.html#ref-list-1